Low-Noise Active Cancellation of Transmitter Leakage and Transmitter Noise in Broadband Wireless Receivers for FDD/Co-Existence

Jin Zhou, *Student Member, IEEE*, Anandaroop Chakrabarti, *Student Member, IEEE*, Peter R. Kinget, *Fellow, IEEE*, and Harish Krishnaswamy, *Member, IEEE*

***Abstract*—A technique for active cancellation of transmitter self-interference in wideband receivers is presented. The active TX leakage cancellation circuitry is embedded within a noise-cancelling low-noise transconductance amplifier (LNTA) so that the noise and the distortion of the cancellation circuitry are cancelled, resulting in a noise-cancelling, self-interference cancelling receiver (NC-SIC RX). A second-point cancellation of TX noise in the RX band is performed after the LNTA so that the noise impact of the second canceller is reduced. Theoretical analyses related to the benefits and limits of active self-interference cancellation as well as the simultaneous cancellation of the noise and distortion of the cancellation circuitry are presented. A 0.3–1.7 GHz receiver with the proposed active cancellation is implemented in 65 nm CMOS. The proposed scheme can cancel up to +2 dBm peak TX leakage at the receiver input. The triple beat at +2 dBm peak TX leakage is 68 dB and the effective IIP3 is +33 dBm, representing increases of 38 and 19 dB, respectively, over the receiver without cancellation. The associated increase in receiver NF is less than 0.8 dB. In addition, the scheme effectively suppresses TX noise in RX band by up to 13 dB. The technique can be more generally viewed as an active combining structure that has ideally no noise penalty and is able to handle large signals without generating distortion and can be applied to any scenario where a replica of an interference signal can be generated.**

***Index Terms*—Blocker, CMOS, co-existence, cross-modulation, FDD, noise-cancelling, receiver, SAW-less, self-interference, transmitter leakage, transmitter noise in receiver band, triple beat, wideband.**

I. Introduction

A major trend in wireless communication systems is the investigation of radio-frequency (RF) transceivers that can be widely tuned across frequency bands. However, wideband receiver front-ends have to handle interference signals that are much larger than those in conventional narrowband receivers due to the lack of tunable high-Q front-end RF filters.

Various techniques have been proposed to cope with out-of-band (OOB) blockers in wideband receivers, and typically focus on 0 dBm continuous-wave (CW) blockers as prescribed in wireless communication standards. These include integrated tunable N-path filters [1]–[7], mixer-first receivers [8]–[10], current-mode receivers [11]–[15], and feed-forward/feedback interference cancellation using translational loops or N-path filters [16]–[20]. While these blocker-management techniques are promising, the continuous drive for a reduction of system form-factor results in lower isolation among antennas due to the co-existence of multiple transceivers within the same compact mobile platform or lower isolation within duplexers for frequency-division duplexing (FDD) systems due to their reduced size and/or increased reconfigurability [21] (Fig. 1). *For the same power level, OOB modulated transmitter self-interference (or TX leakage) due to reduced antenna/duplexer isolation imposes challenges that are more severe than those posed by continuous-wave (CW) blockers by several orders of magnitude, including cross-modulation, second-order inter-modulation and TX noise in the receiver (RX) band.* A detailed system-level analysis is presented in Section II, but the aforementioned blocker-management techniques exhibit insufficient OOB linearity to meet these requirements. In addition, they do not address the issue of TX noise in the RX band.

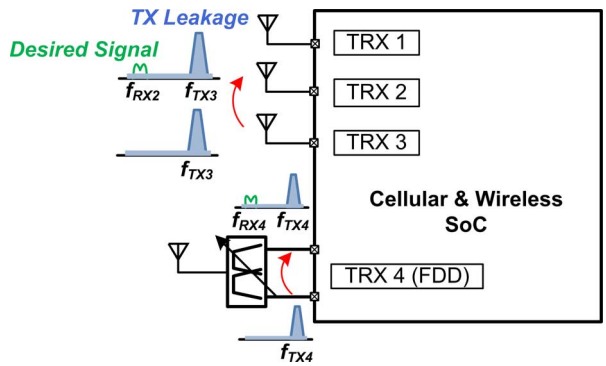

Fig. 1. Mechanisms of transmitter self-interference in a compact mobile platform.

However, knowledge of the self-interference signal enables cancellation-based architectures where a portion of the TX signal is coupled from the TX and subtracted at the RX. TX leakage cancellation may be pursued using passive or active circuitry. Passive TX leakage suppression requires bulky LC-based or transmission line-based [22] cancellation paths that are not amenable to silicon integration and wideband/tunable operation. Absence of some gain in the cancellation path

Manuscript received May 05, 2014; revised August 06, 2014; accepted September 03, 2014. Date of publication October 13, 2014; date of current version November 20, 2014. This paper was approved by Guest Editor Sven Mattisson. This work was supported by the DARPA RF-FPGA program.

The authors are with the Department of Electrical Engineering, Columbia University, New York, NY 10027 USA (e-mail: harish@ee.columbia.edu).

Color versions of one or more of the figures in this paper are available online at http://ieeexplore.ieee.org.

Digital Object Identifier 10.1109/JSSC.2014.2359914

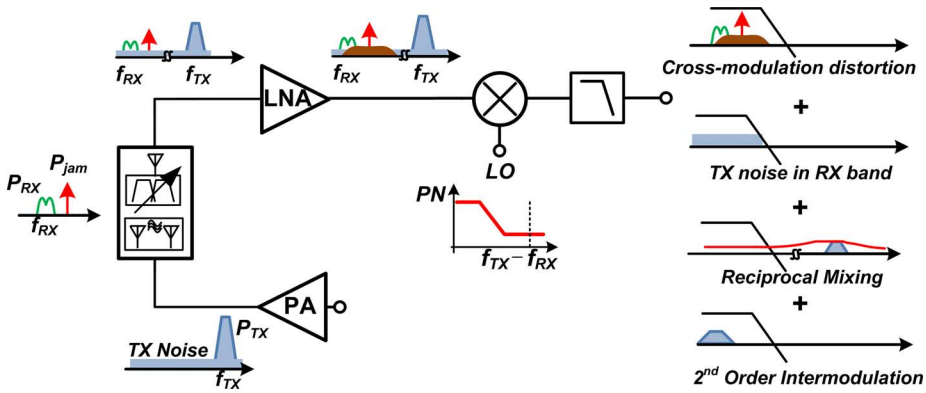

Fig. 2. Receiver challenges in the presence of strong transmitter self-interference.

also prevents support for antenna interfaces with low inherent isolation due to inevitable losses in coupling a replica signal out of the TX and into the RX and in the canceller itself. Active TX leakage filtering and cancellation techniques [23]–[26] have been proposed, but they typically do not relax the LNTA input linearity requirement and/or are limited to leakage levels of -25 to -28 dBm as they assume a commercial (fixed-frequency) duplexer with >50 dB isolation.

The fundamental challenge associated with active TX self-interference cancellation is the degradation of RX performance due to the noise and distortion of the active devices, particularly when designed to handle powerful self-interference and performed at the RX input. A technique for reconfigurable low-noise active cancellation of modulated TX self-interference as high as $+2$ dBm in wideband receivers was presented in [27], enabling FDD/co-existence with as low as 25 dB TX-RX isolation. The active TX leakage cancellation circuitry is embedded within a noise-cancelling low-noise transconductance amplifier (LNTA) so that the noise and the distortion of the cancellation circuitry are cancelled. The result is a noise-cancelling, self-interference cancelling receiver (NC-SIC RX). A second-point cancellation of TX noise in the RX band is performed after the LNTA so that the noise impact of the second canceller is reduced. Section II discusses system-level analyses of transceiver requirements under reduced TX-RX isolation, the tradeoffs and benefits associated with active cancellation, and the TXRR limitations imposed by the frequency selectivity of the antenna interface. Section III describes the proposed low-noise TX leakage cancellation technique as well as an analysis of simultaneous cancellation of the noise and distortion of the cancellation circuitry. Sections IV and V discuss circuit implementations and measurement results, respectively. Section VI concludes the paper.

II. System-Level Analysis of Active Cancellation

A. System Requirements Under Reduced TX-RX Isolation

Fig. 2 depicts a simplified direct-conversion receiver front-end detecting a weak signal P_{RX}. The output of a transmitter on the same platform couples to the receiver input through the antenna interface. The transmitter generates a powerful signal P_{TX} that is outside the RX band as well as a noise floor that extends to the RX band. The TX leakage can degrade the receiver performance in several ways (Fig. 2). In this work, we focus on cross-modulation distortion and TX noise in the RX band. The TX leakage can cross-modulate with an in-band CW jammer (P_{jam} in Fig. 2), desensitizing the receiver [28], [29]. Modeling the transmitter signal as two tones, the input-referred cross-modulation product can be calculated as [30]

$$P_{\mathrm{xmod,in}} = 2(P_{\mathrm{TX,avg}} - \mathrm{ISO}) - 2\mathrm{IIP}_3 + P_{\mathrm{jam}} \qquad (1)$$

where $P_{\mathrm{TX,avg}}$ is the average transmitted power, ISO is the TX-RX isolation, and IIP_3 is the receiver OOB input-referred third-order intercept point. Note that all quantities are expressed in dB scale. We assume a desired SNR of 7 dB, signal bandwidth of 2 MHz, in-band jammer power of -30 dBm and peak PA output power of $+24$ dBm. For a receiver with 5 dB NF, the sensitivities based on the individual contributions of cross-modulation distortion and TX noise in the RX band are plotted in Fig. 3. For 55 dB isolation, offered by current fixed-frequency duplexers, OOB IIP_3 of $+10$ dBm is sufficient for -100 dBm sensitivity. However, for a reduced isolation of 25 dB, enabling low-cost/compact/tunable front-end modules, receiver OOB IIP_3 greater than $+30$ dBm is required. A stringent requirement of -170 dBc/Hz is seen for the RX-band TX noise as well.

B. Tradeoffs and Benefits Associated With Active TX Leakage Cancellation

As mentioned earlier, knowledge of the self-interference signal enables TX leakage cancellation architectures. Active TX leakage cancellation has the advantages of being area efficient, more amenable to silicon integration and widely tunable when compared with passive leakage cancellation approaches. Furthermore, the presence of some gain in the cancellation path enables cancellation across antenna interfaces with low inherent isolation. At the same time, the noise and distortion added by the active circuitry must be considered. A natural question is whether the active canceller dc power consumption may be used in the original receiver to achieve equivalent performance. These topics are analyzed in detail in this section.

A generic active TX leakage cancellation approach is shown in Fig. 4(a), where a portion of the TX signal is coupled from the power amplifier (PA) output. The TX replica signal is then adjusted in amplitude and phase, and subtracted at the RX

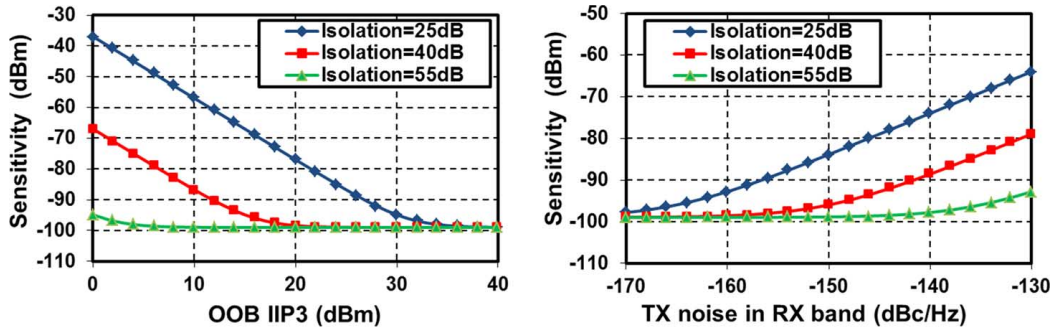

Fig. 3. Receiver sensitivity with varying TX-RX isolation for different (a) out-of-band IIP3 levels and (b) levels of TX noise in RX band. Desired SNR of 7 dB, signal BW of 2 MHz, an in-band CW jammer power of −30 dBm, peak PA output power of +24 dBm and RX NF of 5 dB are assumed.

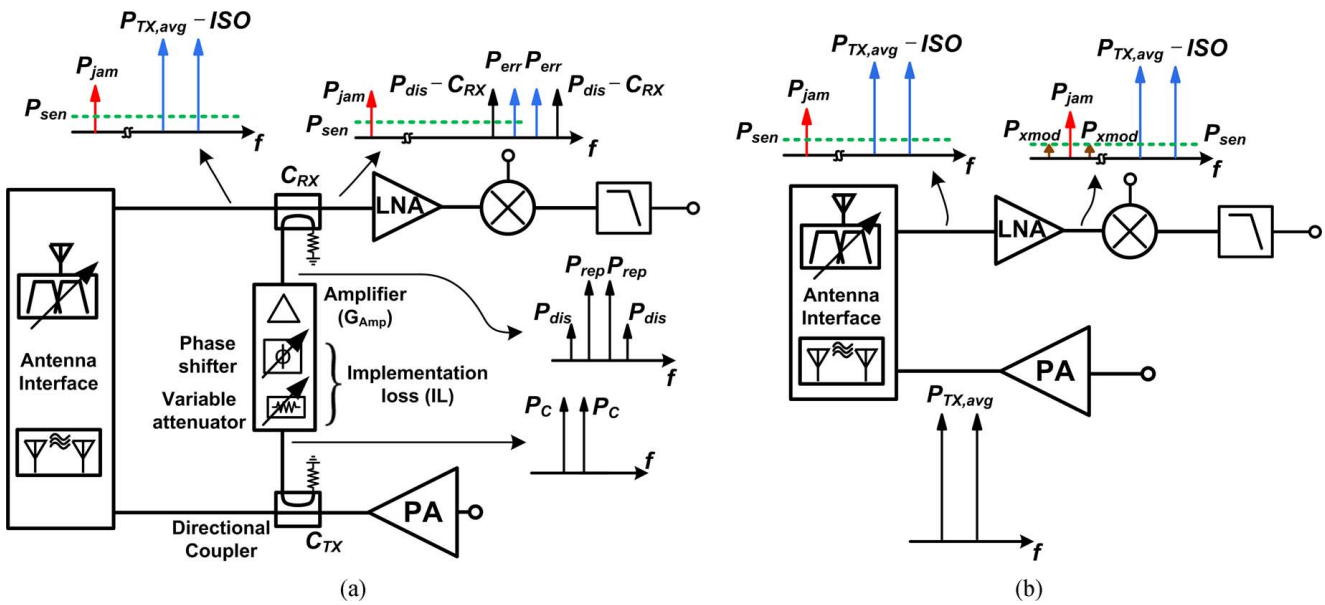

Fig. 4. Transceiver block diagram with two-tone TX leakage signal along with an in-band CW jammer at the input of the receiver: (a) with a generic active TX-leakage canceller and (b) without TX-leakage cancellation.

input using another coupler. To partially compensate for the coupling ratios of the couplers ($C_{\rm TX}$ and $C_{\rm RX}$) and implementation losses (IL) in the canceller, an amplifier with power gain $G_{\rm Amp}$ is used in the canceller. Thus, the total gain of the canceller can be written as $G_{\rm Canceller} = G_{\rm Amp} - IL$. $C_{\rm TX}$ must be high to avoid degrading PA efficiency and is assumed to be 15 dB. The required amplifier gain $G_{\rm Amp}$ can be related to ISO in the dB scale as

$$\mathrm{ISO} = C_{\rm TX} + C_{\rm RX} - G_{\rm Canceller} = C_{\rm TX} + C_{\rm RX} - G_{\rm Amp} + IL. \quad (2)$$

If the noise figures of the canceller and the RX are $\mathrm{NF}_{\rm Canceller}$ and $\mathrm{NF}_{\rm RX}$, respectively, the NF of the RX including the canceller can be calculated as

$$\mathrm{NF}_{\rm RX,tot} = 10\log_{10}(10^{NF_{\rm RX}/10} + 10^{(\mathrm{NF}_{\rm Canceller} + G_{\rm Amp} - IL - C_{\rm RX})/10}). \quad (3)$$

From (3) and (2), a larger value of $C_{\rm RX}$ protects the receiver from NF degradation due to the canceller but requires greater ISO to be achieved in the antenna interface. Assuming $\mathrm{NF}_{\rm RX} = 3$ dB, $\mathrm{NF}_{\rm Canceller} = 12$ dB, $C_{\rm TX} = 15$ dB, $C_{\rm RX} = 10$ dB, $IL = 5$ dB, the $\mathrm{NF}_{\rm RX,tot}$ and ISO are plotted versus $G_{\rm Amp}$ in Fig. 5(a). In order to support antenna interfaces with as low as 25–20 dB isolation (for instance, the miniature circulator in [31]), 5–10 dB gain is required in the canceller amplifier but the overall NF will degrade by 2.5–5.5 dB. *Our work breaks this trade-off between support for low antenna interface isolation levels (or equivalently, power of TX leakage being cancelled) and NF degradation through the insight that an active canceller that is integrated with the RX on the RFIC can be co-designed with the RX – by embedding the canceller within the noise-cancelling LNTA, the noise of the cancellation path is cancelled.*

Active TX leakage cancellation at the input of the receiver can relax the receiver linearity requirement but the distortion of the active canceller must be considered. Consider a receiver without TX leakage cancellation in Fig. 4(b) and assume a two-tone signal for the TX signal. Using (1) and assuming that the receiver is sufficiently linear to keep the cross-modulation

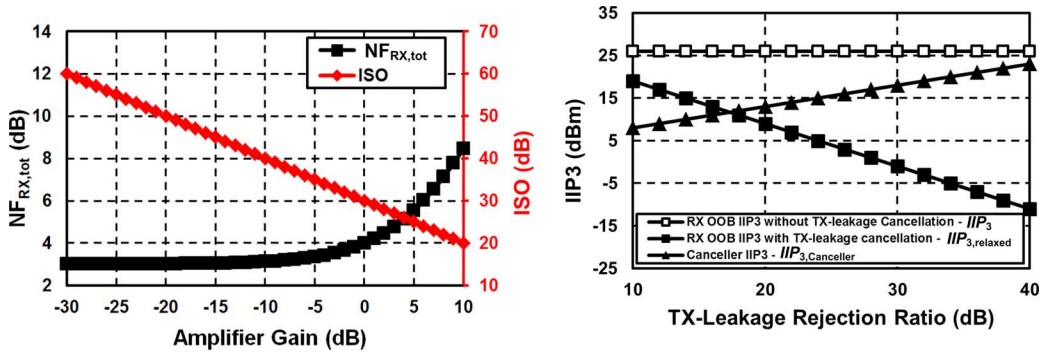

(a) (b)

Fig. 5. (a) Total RX NF and minimum supported inherent antenna interface isolation as a function canceller amplifier gain ($IL = 5$ dB, $C_{\rm RX} = 10$ dB, $C_{\rm TX} = 15$ dB, $\rm NF_{RX} = 3$ dB, $NF_{\rm Canceller} = 12$ dB). (b) Required RX OOB IIP3 with/without TX leakage cancellation and required canceller IIP3 ($P_{\rm TX,avg} = +21$ dBm, $\rm ISO = 25$ dB, $IL = 5$ dB, $G_{\rm Amp} = 5$ dB, $C_{\rm RX} = 10$ dB, $C_{\rm TX} = 15$ dB, $P_{\rm jam} = -30$ dBm, and $P_{\rm sen} = -90$ dBm).

distortion products at the receiver sensitivity level, the required OOB $\rm IIP_3$ is

$$\rm IIP_3 = (P_{TX,avg} - ISO) + \frac{1}{2}(P_{jam} - P_{sen}) \quad (4)$$

where $P_{\rm sen}$ is the receiver sensitivity and we have assumed that only one of the two cross-modulation tones falls on top of the desired signal.

Now, consider a receiver with an active TX leakage canceller shown in Fig. 4(a). The finite linearity of the canceller will generate third-order intermodulation tones at the receiver input. These intermodulation tones as well as the residual TX leakage due to finite TX leakage cancellation can still cross-modulate with the jammer. The canceller should have sufficient linearity to keep the distortion tones at the level of the residual TX leakage signal—a further increase in the canceller power consumption would not help, since the sensitivity would dominated by cross modulation products generated by the residual TX leakage. The extent of TX leakage cancellation is limited by the selectivity of the antenna interface leakage path (amplitude, phase and group delay variation with frequency) [25]. This is quantified in the following subsection. Nevertheless, with these design guidelines, the canceller $\rm IIP_3$ is

$$\begin{aligned}&\rm IIP_{3,Canceller}\\ &= P_C + \frac{1}{2}(P_{\rm rep} - P_{\rm dis})\\ &\approx P_{\rm TX,avg} - \rm ISO - 3 + C_{RX} - G_{Canceller} + \frac{\Delta}{2}\end{aligned} \quad (5)$$

where P_C is the coupled signal power from the PA at the input of the canceller, $P_{\rm rep}$ is the replica TX leakage power at the output of the canceller, and $P_{\rm dis}$ is the power of the third-order distortion produced by the canceller. Each of them represents the power of one tone of a two-tone signal. We have assumed that the cancellation signal has approximately the same power as the TX leakage ($P_{\rm rep} \approx P_{\rm TX,avg} - \rm ISO - 3 + C_{RX}$). The power gain of the canceller $G_{\rm Canceller} = P_{\rm rep} - P_C$, and consequently $P_C \approx P_{\rm TX,avg} - \rm ISO - 3 + C_{RX} - G_{Canceller}$. $\Delta = P_{\rm TX,avg} - \rm ISO - 3 - P_{err}$ is the TXRR in dB scale. The canceller is designed so that the third-order distortion tone at the RX input ($P_{\rm dis} - C_{\rm RX}$) is equal to the residual TX leakage ($P_{\rm err}$). Therefore, we have $\Delta \approx P_{\rm rep} - P_{\rm dis}$.

At the same time, the relaxed receiver OOB $\rm IIP_3$ after the TX-leakage cancellation is

$$\rm IIP_{3,relaxed} = P_{TX,avg} - ISO - \Delta + 3 + \frac{1}{2}(P_{jam} - P_{sen}). \quad (6)$$

The additional 3 dB in (6) comes from the cross-modulation distortion produced by $P_{\rm dis}$.

It can be seen that a larger value of $C_{\rm RX}$ requires the canceller to handle higher power levels and exhibit higher linearity. Given $P_{\rm TX,avg} = +21$ dBm, $\rm ISO = 25$ dB, $G_{\rm Amp} = 5$ dB, $IL = 5$ dB, $C_{\rm RX} = 10$ dB, $P_{\rm jam} = -30$ dBm and $P_{\rm sen} = -90$ dBm, we plot (4)–(6) as a function of TXRR in Fig. 5(b). In Fig. 5(b), the calculated receiver OOB $\rm IIP_3$ without TX leakage cancellation is $+26$ dBm, while, with a TXRR of 20 dB, the receiver OOB $\rm IIP_3$ is relaxed to $+9$ dBm and the canceller $\rm IIP_3$ must be $+13$ dBm.

Given that modern wideband high-linearity receivers often implement some form of blocker filtering right after the LNA, the receiver OOB $\rm IIP_3$ can be assumed to be dominated by the (wideband) $\rm IIP_3$ of the LNA. Consequently, a fair comparison can be made between the dynamic range requirement and power consumption of the LNA with and without cancellation and those of the amplifier in the active canceller. The canceller design itself is typically a trade-off between noise performance and linearity. Since linearity is typically challenging to achieve in scaled CMOS, one may assume that the (lossy) attenuator and phase shifter precede the amplifier in the canceller to alleviate its linearity requirement. In other words, assuming that the $IL = 5$ dB precedes the gain, the noise figure of the amplifier $\rm NF_{amp}$ to meet the $\rm NF_{canceller} = 12$ dB assumption made earlier is 7 dB. The amplifier IIP_3 requirement in the canceller becomes $+8$ dBm. Therefore, the RX LNA in the absence of cancellation must exhibit an NF of 5.5 dB and a wideband $\rm IIP_3$ of $+26$ dBm to match the performance of an active cancellation scheme where the RX LNA exhibits $\rm NF = 3$ dB and a wideband $\rm IIP_3$ of $+9$ dBm and the amplifier in the canceller exhibits $\rm NF = 7$ dB and a wideband $\rm IIP_3$ of $+8$ dBm. It is clear that the combination of a receiver and a TX leakage canceller consumes much less power than a receiver alone that is designed

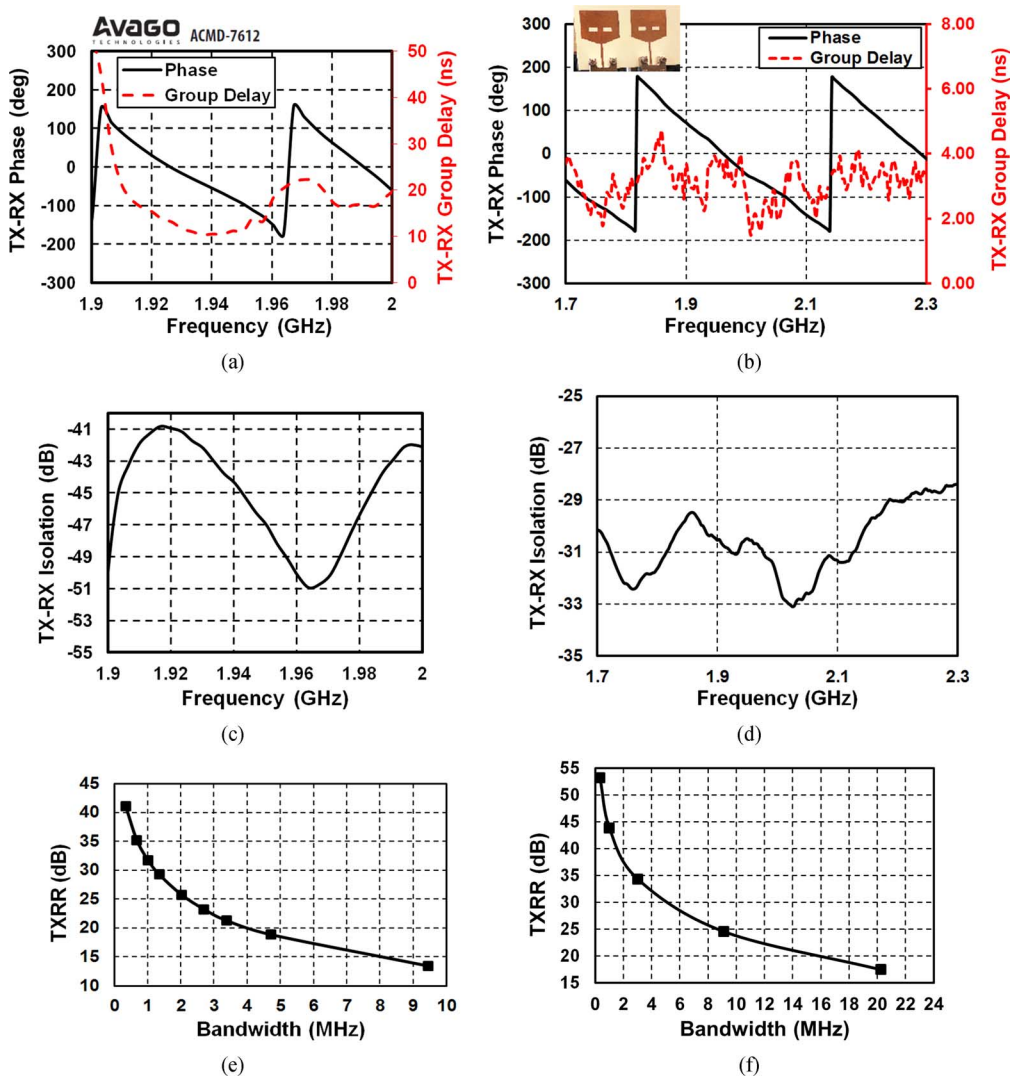

Fig. 6. Measured isolation phase and group delay of the (a) Avago ACMD-7612 miniature UMTS band-I duplexer and (b) a wideband PCB antenna pair. Measured isolation magnitude response of the (c) Avago duplexer and (d) the wideband PCB antenna pair. Calculated maximum achievable TXRR versus TX signal BW assuming an OFDM signal with 50 subcarriers and constant phase and amplitude scaling from the canceller for the (e) Avago duplexer and (f) the wideband PCB antenna pair.

to handle the TX leakage. This is because the TX leakage canceller dramatically relaxes the receiver linearity requirement. While the canceller has to handle a large replica signal, it has a significantly lower dynamic range requirement than a receiver without leakage cancellation as it does not handle the weak desired signal. Hence its distortion does not need to be below the sensitivity level. Another advantage of active cancellation is that the canceller can be deactivated to save power when the TX is off or operating at low output power levels.

While active cancellation is necessary to support low isolation levels, enables compact, wideband implementations, and significantly relaxes the power consumption of the entire system, the design of the canceller does feature a trade-off between noise and linearity. The analysis just presented applies to generic active cancellation. *Our work, however, breaks this tradeoff—as will be seen in the following sections, the canceller is embedded in the RX's noise-cancelling LNTA, effectively eliminating* C_{RX}. *The strong coupling into the receiver significantly relaxes the canceller linearity requirement, and the associated NF penalty is not seen due to the cancellation of the noise of the canceller.*

C. Limits on Cancellation Bandwidth for Active/Passive TX Leakage Cancellation

TXRR is limited by the amplitude and phase resolution of the canceller as well as the selectivity of the antenna interface[25]. The former can be high in scaled CMOS processes, but the latter depends on the nature of the antenna interface and typically dominates cancellation bandwidth (BW). Fig. 6(b) and (d) depicts measurements of the isolation phase and magnitude of a wideband PCB-based antenna pair [32], revealing a broadband isolation magnitude with around 3 ns group delay. Using these responses, the maximum achievable TXRR for an OFDM signal with 50 sub-carriers given a broadband amplitude and phase response from the canceller is calculated and plotted versus TX signal BW in Fig. 6(f). A broadband canceller is useful for signals with up to 15 MHz BW assuming 20 dB cancellation is required. To further demonstrate the impact of

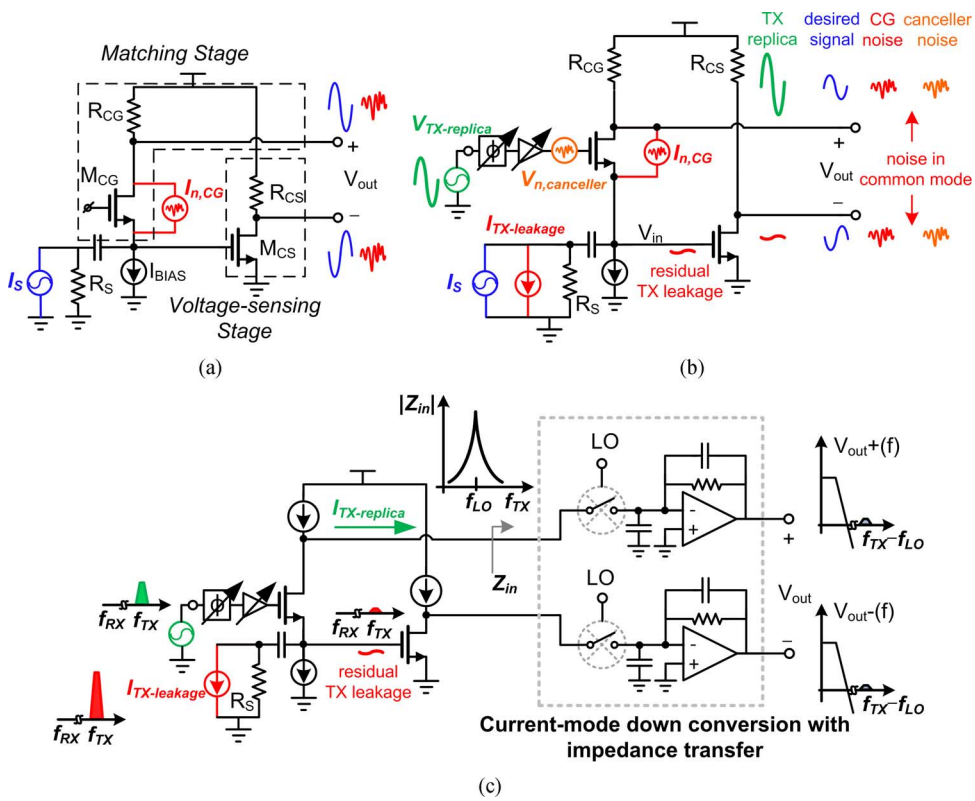

Fig. 7. Evolution of the proposed NC-SIC RX. (a) Noise-cancelling LNA in [34]. (b) Noise-cancelling LNA with embedded TX leakage cancellation. (c) NC-SIC RX with current-mode downconversion to alleviate the output-side linearity challenge in the CG path.

the antenna interface on the TX leakage cancellation BW, isolation phase and magnitude responses of an Avago ACMD-7612 miniature UMTS band-I duplexer [33] were also measured [Fig. 6(a) and (c)] in the TX band (1.9–2 GHz), revealing a isolation magnitude that varies from 40 to 50 dB with around 20 ns group delay. It should be noted that the Avago duplexer already has high isolation and therefore does not require cancellation. Our technique is intended to relax duplexer isolation requirements, reducing the filter order and the duplexer selectivity and therefore enabling wider cancellation BWs. Nevertheless, the selectivity of the Avago duplexer limits the 20 dB TXRR BW to 4 MHz at the band center [Fig. 6(e)]. Small-signal TXRR measurements across the TX passband of this duplexer with our prototype receiver are presented in Section V.

III. Proposed TX Leakage and TX Noise-Cancelling Receiver

A. Embedding TX Leakage Cancellation in a Noise-Cancelling Current-Mode Receiver

The concept of noise cancelling in wideband LNAs uses a voltage-sensing stage [the common-source (CS) transistor $M_{\rm CS}$ shown in Fig. 7(a)] in addition to a matching stage [common-gate (CG) transistor $M_{\rm CG}$ in Fig. 7(a)] so that when the outputs of the two stages are combined (differentially in this case), the noise from the matching device adds destructively while the desired signals are added constructively [34]–[36]. The condition to cancel the common-gate device's noise and generate a balanced desired signal at the LNA output is

$$g_{m,\rm CG}R_{\rm CG} = g_{m,\rm CS}R_{\rm CS} \tag{7}$$

where we have assumed that $g_{m,\rm CG}R_S = 1$ for input matching.

The proposed TX leakage cancellation technique [27] repurposes the CG device as part of the TX leakage canceller as in Fig. 7(b). By driving the gate of the CG device with an appropriately scaled TX replica signal, the leakage can be cancelled *right at the input of the LNA*. A TX-replica signal is injected at the gate of the CG device through a phase shifter and VGA, while the desired signal and the TX leakage are both present at the LNA input.

Applying KCL at the LNA input and considering only the TX leakage, we have

$$g_{m,\rm CG}(A_{\rm canceller}V_{\rm TX-replica} - V_{\rm in}) = I_{\rm TX-leakage} + \frac{V_{\rm in}}{R_S} \tag{8}$$

where $A_{\rm canceller}$ is the voltage gain of the phase shifter and VGA. If the VGA and phase shifter are adjusted so that $g_{m,\rm CG}A_{\rm canceller}V_{\rm TX-replica} = I_{\rm TX-leakage}$, then $V_{\rm in} = 0$, indicating the TX-leakage voltage swing is eliminated at the LNA input. It is interesting to note that, under TX-leakage cancellation, the source node of the CG device is a virtual ground for the TX-replica signal, and therefore the CG device is not degenerated by the source resistance.

Meanwhile, interestingly, the entire noise from the active canceller, namely the transistor $M_{\rm CG}$, variable-gain amplifier

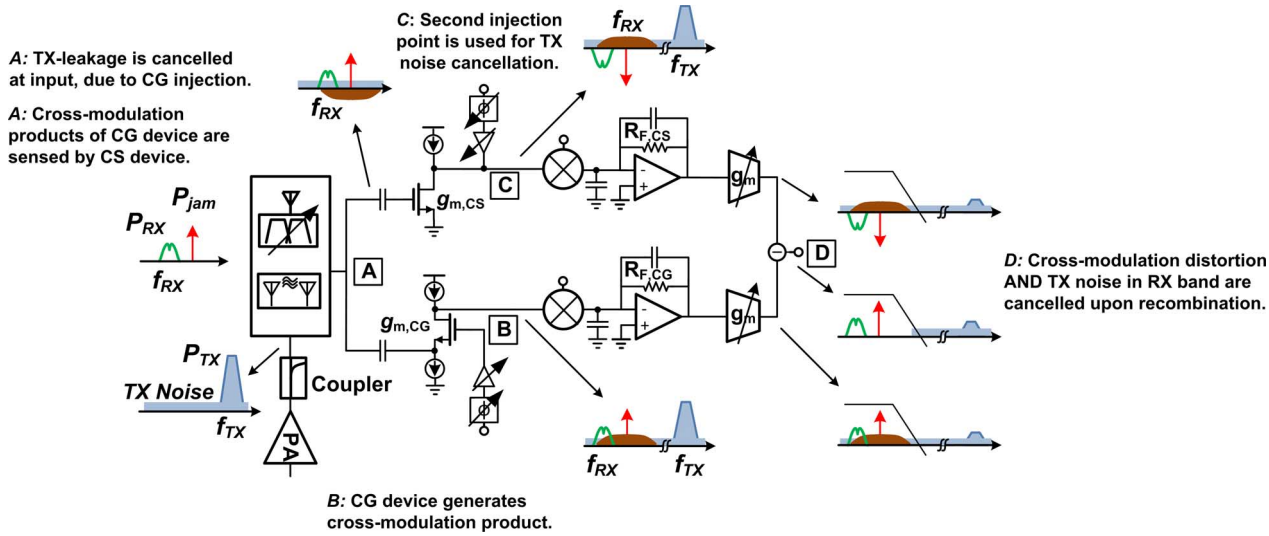

Fig. 8. Cancellation of the cross-modulation distortion of the CG device in the proposed NC-SIC RX, and the second injection point in the CS path for RX-band TX noise cancellation.

and phase shifter, gets completely cancelled through the noise cancelling property, as the common source device $M_{\rm CS}$ senses the noise from the canceller and then subtracts it at the output. Therefore, in the proposed scheme, TX leakage cancellation is achieved right at the LNA input with ideally no noise penalty, while the desired signal appears differentially at the LNA output. A detailed noise analysis will be presented in the next subsection.

While the leakage is cancelled at the input, a large leakage current still flows down the CG device producing a large voltage swing ($I_{\rm TX-leakage}R_{\rm CG}$) at its output. To mitigate this, in Fig. 7(c), a current-mode down conversion stage with impedance transfer from baseband consisting of passive mixers and baseband transimpedance amplifiers (TIAs) is inserted before the combining network to filter out the large OOB leakage current before the achievement of voltage gain. The structure has evolved into a NC-SIC RX.

While the LNTA CS device is protected due to the leakage cancellation at the input, the CG device still experiences large voltage swing at its gate node due to the CG canceller injection, and can generate cross-modulation distortion together with an incident in-band CW jammer. The cross-modulation distortion generated by the CG device appears at the input as well as in the CG path of the receiver as depicted in Fig. 8. *Interestingly, in the proposed scheme, the cross-modulation distortion of the CG device gets cancelled as well upon baseband recombination, as the cross-modulation distortion is sensed by the CS device, generating a distortion current that is in phase with the distortion current in the CG path*. This is similar to the distortion cancellation property of noise-cancelling LNAs [35], [37] and implies that *TX leakage cancellation has been achieved with no noise or distortion penalty*.

It is interesting to take a more general view of the proposed scheme as an active combining circuit that has ideally no noise penalty, and is able to handle large signals without generating distortion. Consequently, the scheme can be used to cancel any interference signal for which a replica can be generated.

Cancellation of the TX leakage at the RX input does not guarantee cancellation of the RX-band TX noise at the input, as their transfer functions through the antenna interface will be different. Consequently, the TX noise remains in both the CG and CS paths, and can desensitize the receiver. Since noise is small, TX noise can be cancelled down the receiver chain [38]. A second injection point is introduced in current mode at the output of the CS device (Fig. 8). With appropriate scaling using the CS canceller, TX noise can be nulled upon baseband recombination. The noise penalty of the CS canceller is alleviated by the CS gain. At this second injection node, the main TX-band signal is injected together with the RX-band TX noise, and flows down the receiver CS down-conversion path. This main TX-band signal is filtered out in the baseband TIAs, and current mode design mitigates the potential linearity issues caused by it.

The TX-band leakage currents flowing down the CG and CS paths to baseband can degrade receiver performance through mixer impairments such as the generation of IM2 products. It should be noted that these leakage currents are similar to the currents in these paths in the absence of cancellation. IM2 challenges can be mitigated through mixer calibration techniques [39], [40].

B. Noise Analysis of the Noise and Leakage-Cancelling Receiver

Here, the noise performance of the NC-SIC RX is analyzed. A subtle mechanism of NF penalty is revealed, produced by the fact that the optimal baseband recombination condition for cancellation of the CG canceller noise is different from the condition that minimizes receiver NF in the absence of leakage cancellation circuitry. The CS canceller noise contribution is not included in the noise analysis, since the CS canceller is only activated when TX noise in the RX band dominates. Furthermore, since noise is a small-signal, TX noise cancellation can be performed further down the receiver chain, minimizing the noise impact even further.

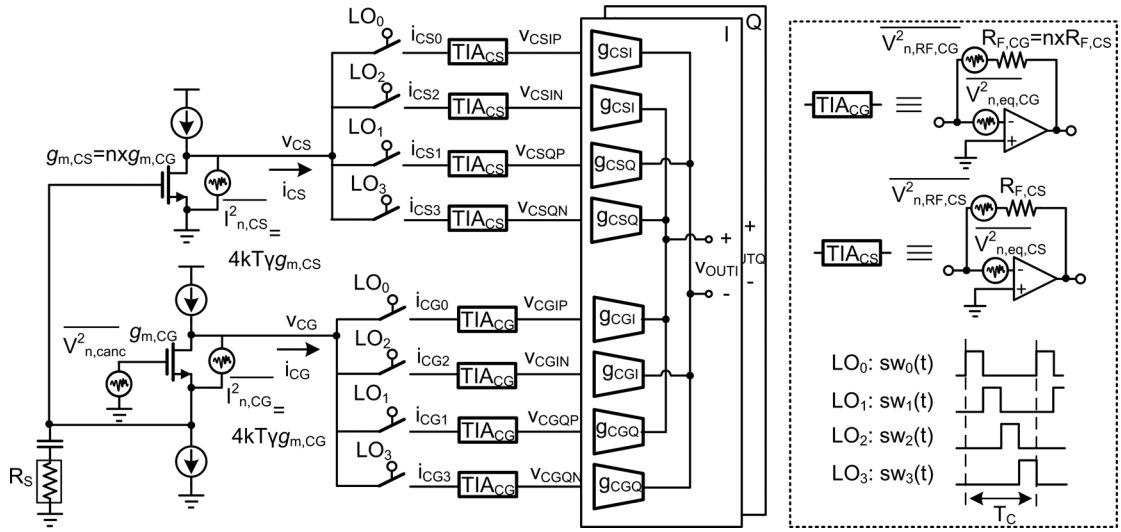

Fig. 9. Noise analysis model for the NC-SIC RX.

Based on the noise model in Fig. 9, the noise figure (NF) for the entire receiver is given by (9), shown at the bottom of the page, where $K_{\rm Fold} \approx$ 0.9 dB is a constant that factors in the noise folding effect of 4-phase mixing, $\delta = g_{\rm CGI}/g_{\rm CSI}$ is the ratio between the recombination weights on receiver's CG and CS paths, $\overline{V^2_{n,\rm canc}}$ is the output noise of the CG canceller, and $\overline{V^2_{n,\rm eq,CG}}$ and $\overline{V^2_{n,\rm eq,CS}}$ are the input-referred noise of the OTAs. The noise has been computed at the output $v_{\rm OUTI}$. Also, $g_{\rm CSQ}$ and $g_{\rm CGQ}$ are assumed to be zero for a purely resistive source impedance. Complex recombination weights may be required to compensate for complex source impedance and other sources of signal path phase-shift differences between the CS and CG paths but such cases are not considered here for simplicity. Note that the weighting to compensate for the ratio of the LNTA CG and CS device transconductance has been performed in baseband TIAs ($R_{F,\rm CG} = n \times R_{F,CS}$ where $n = g_{m,\rm CS}/g_{m,\rm CG}$). The NF in (9) includes three contributors: the CG device and CG canceller noise, CS device noise and the noise of the TIAs. Fig. 10 depicts the calculated and simulated NF when the canceller is inactive ($\overline{V^2_{n,\rm canc}} = 0$) across δ. The simulations presented in this section are for the actual receiver implementation described in the following subsection at 500 MHz LO frequency, but without layout parasitics to ease simulation time and with ideal mixer switches and LO drive. Hence, the final performance numbers are close to the measured values but are slightly lower. As indicated by (9), the noise from the CG device gets cancelled

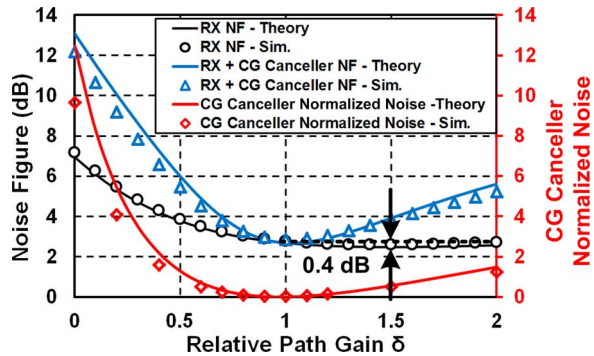

Fig. 10. Receiver NF with and without the CG canceller active and normalized CG canceller noise as a function of the (real) relative path gain setting in the baseband recombination block. Markers depict simulation results for the actual receiver implementation at 500 MHz LO frequency. Solid lines depict theoretical results calculated using (9).

when relative path gain $\delta = R_S g_{m,\rm CS} R_{F,CS}/R_{F,\rm CG} = 1$ (assuming $g_{m,\rm CG} R_S = 1$ for input matching). However, the optimum relative path gain for the receiver NF is around 1.5 in Fig. 10 as this optimizes the contributions from other noise sources ([37]), including the CS device and baseband TIAs. On the other hand, the CG canceller noise ($\overline{V^2_{n,\rm canc}}$) still gets cancelled when the δ equals 1 as is indicated by the CG canceller normalized noise (i.e., CG canceller NF component, calculated as the noise contribution from the canceller divided by that from

$$\mathrm{NF} = K_{\rm Fold}\left[1 + \frac{(R_{F,\rm CG}\delta - R_S g_{m,\rm CS} R_{F,\rm CS})^2\left(\gamma g_{m,\rm CG} + \overline{V^2_{n,\rm canc}}\frac{g^2_{m,\rm CG}}{4kT}\right) + \gamma g_{m,\rm CS} R^2_{F,\rm CS}(1 + g_{m,\rm CG} R_S)^2}{(g_{m,\rm CG} R_{F,\rm CG}\delta + g_{m,\rm CS} R_{F,\rm CS})^2 R_S}\right]$$
$$+ \pi^2 \frac{(1 + g_{m,\rm CG} R_S)^2\left[\left(4kTR_{F,\rm CG} + \overline{V^2_{n,\rm eq,CG}}\right)\delta^2 + 4kTR_{F,\rm CS} + \overline{V^2_{n,\rm eq,CS}}\right]}{4kT(g_{m,\rm CG} R_{F,\rm CG}\delta + g_{m,\rm CS} R_{F,\rm CS})^2 R_S} \quad (9)$$

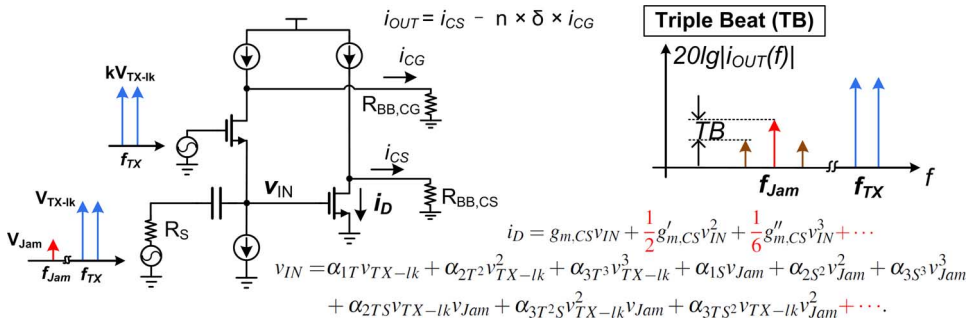

Fig. 11. Circuit model for the analysis of cross-modulation distortion in the NC-SIC LNTA in the presence of the TX leakage and an in-band CW jammer.

the source impedance R_S) in Fig. 10. Therefore, when CG canceller is active, the relative path gain δ is very close to 1, as the noise from the CG canceller dominates. This change in the optimal baseband recombination condition is an indirect source of NF penalty in the proposed scheme. However, the resultant NF penalty is only 0.3–0.4 dB in Fig. 10.

C. Simultaneous Cancellation of CG Noise and Cross-Modulation Distortion

As was discussed earlier, the noise canceling architecture also cancels the distortion of the CG device. As depicted in Fig. 11, in order to perform the LNTA linearity analysis under TX leakage cancellation, two excitations are included—one at the input of the LNTA containing the leakage $v_{\mathrm{TX-lk}}$ and the jammer signal v_{Jam}, and the other at the gate of the LNTA CG device containing a scaled TX replica signal. To model the CG device nonlinearity, we expand the input voltage v_{IN} into a 2-variable power series of the leakage and the jammer signals as follows:

$$\begin{aligned} v_{\mathrm{IN}} = {} & \alpha_{1T}v_{\mathrm{TX-lk}} + \alpha_{2T^2}v_{\mathrm{TX-lk}}^2 + \alpha_{3T^3}v_{\mathrm{TX-lk}}^3 \\ & + \alpha_{1S}v_{\mathrm{Jam}} + \alpha_{2S^2}v_{\mathrm{Jam}}^2 + \alpha_{3S^3}v_{Jam}^3 \\ & + \alpha_{2TS}v_{\mathrm{TX-lk}}v_{\mathrm{Jam}} + \alpha_{3T^2S}v_{\mathrm{TX-lk}}^2v_{\mathrm{Jam}} \\ & + \alpha_{3TS^2}v_{\mathrm{TX-lk}}v_{\mathrm{Jam}}^2 + \cdots. \end{aligned} \tag{10}$$

The device current is assumed to depend (nonlinearly) on gate-source voltage primarily. The first number in the subscripts of the α coefficients represents the order of the nonlinearity arising from the LNTA CG device and the exponents of T and S in the subscripts denote the exponents of the TX leakage and the jammer signal in that term respectively. For instance, α_{3T^2S} arises from the third-order nonlinearity of the CG device and is the coefficient of the $v_{\mathrm{TX-lk}}^2v_{Jam}$ term. To model the CS device nonlinearity, its drain current is expanded into a power series of its gate voltage.

$$i_D = g_{m,\mathrm{CS}}v_{\mathrm{IN}} + \frac{1}{2}g'_{m,\mathrm{CS}}v_{\mathrm{IN}}^2 + \frac{1}{6}g''_{m,\mathrm{CS}}v_{\mathrm{IN}}^3 + \cdots. \tag{11}$$

Memory elements such as capacitive parasitics as well as off-chip biasing inductors and capacitors have been ignored. Consequently, the analysis is valid within the RF bandwidth of the receiver where these memory elements are ineffectual.The output is defined as $I_{\mathrm{CS}} - n \times \delta \times I_{\mathrm{CG}}$ where n is the nominal (real) weighting achieved in the baseband TIAs ($= 4$ in our implementation) and δ is the programmable recombination weighting.

Now, assuming a two-tone signal for the TX leakage (each with amplitude of $A_{\mathrm{TX-lk}}$), the triple beat (TB) [24] is defined as the ratio of the jammer power to the power of the cross-modulation distortion tones in the output as shown in Fig. 11. Circuit analysis along with (10) and (11) can be used to obtain the expression for the LNTA TB given by (12), shown at the bottom of the page.

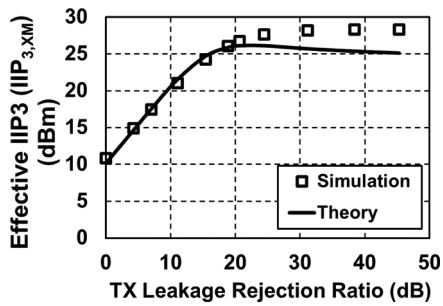

Fig. 12. Effective IIP_3 of the implemented NC-SIC LNTA across TX leakage rejection ratio from simulations and theory. The in-band jammer and the two-tone TX leakage signal (peak power of -6 dBm) are located at 500 MHz and 600/605 MHz, respectively. The TX replica signal at the gate of the CG device is swept to vary TXRR.

$$\begin{aligned} TB^{-1} &\approx \frac{\left[(g_{m,\mathrm{CS}}R_S - n\delta)\alpha_{3T^2S} + g'_{m,\mathrm{CS}}(\alpha_{2T^2}\alpha_{1S} + \alpha_{2TS}\alpha_{1T})R_S + \frac{1}{2}g''_{m,\mathrm{CS}}\alpha_{1T}^2\alpha_{1S}R_S\right]A_{\mathrm{TX-lk}}^2}{2\alpha_{1S}g_{m,\mathrm{CS}}R_S + 2(1-\alpha_{1S})n\delta} \\ &\approx \frac{g'_{m,\mathrm{CS}}\alpha_{2T^2}A_{\mathrm{TX-lk}}^2}{4g_{m,\mathrm{CS}}}, \qquad \text{if } g_{m,\mathrm{CS}}R_S = n\delta,\ \alpha_{1T} = 0 \text{ and } \alpha_{1S} = 0.5 \end{aligned} \tag{12}$$

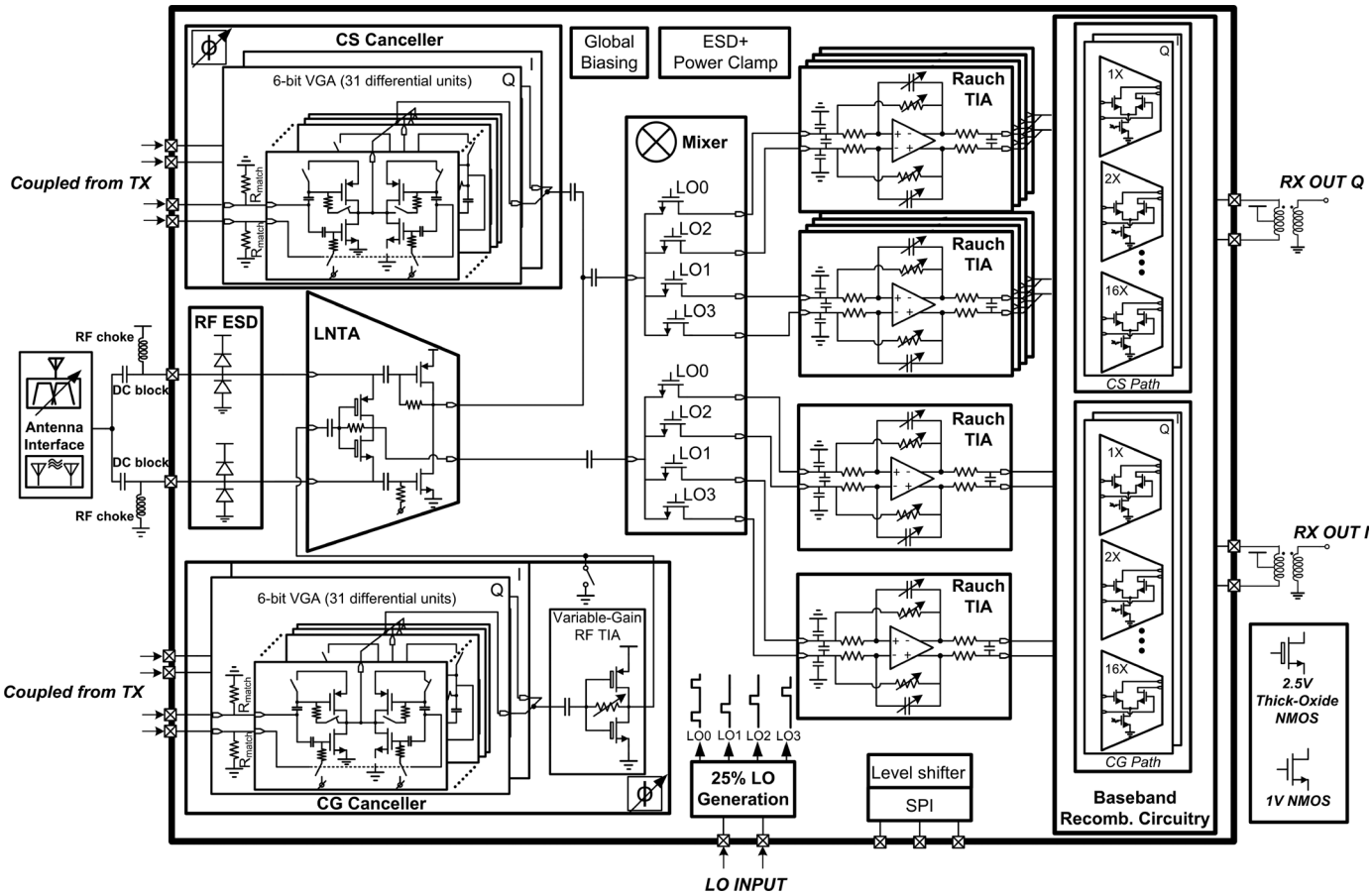

Fig. 13. Block diagram and schematic for the implemented 65 nm CMOS 0.3–1.7 GHz NC-SIC receiver.

The TB has three contributors: third-order nonlinearity of the CG device

$$\left(\frac{(g_{m,\mathrm{CS}}R_S - n\delta)\alpha_{3T^2S}A^2_{\mathrm{TX-lk}}}{2\alpha_{1S}g_{m,\mathrm{CS}}R_S + 2(1-\alpha_{1S})n\delta}\right)$$

third-order nonlinearity of the CS device

$$\left(\frac{\frac{1}{2}g''_{m,\mathrm{CS}}\alpha^2_{1T}\alpha_{1S}R_SA^2_{\mathrm{TX-lk}}}{2\alpha_{1S}g_{m,\mathrm{CS}}R_S + 2(1-\alpha_{1S})n\delta}\right)$$

and an interaction between the second-order nonlinearities of the CG and CS devices

$$\left(\frac{g'_{m,\mathrm{CS}}(\alpha_{2T^2}\alpha_{1S} + \alpha_{2TS}\alpha_{1T})R_SA^2_{\mathrm{TX-lk}}}{2\alpha_{1S}g_{m,\mathrm{CS}}R_S + 2(1-\alpha_{1S})n\delta}\right).$$

The third-order distortion of the CG device gets cancelled upon baseband recombination due to the simultaneous noise and distortion cancellation property of the noise-canceling architecture as indicated in Fig. 8. This corresponds to the condition $g_{m,\mathrm{CS}}R_S = n\delta$ in (12) as $g_{m,\mathrm{CG}} = 1/R_S$ for input matching and $\delta = 1$ for cancellation of the CG device and CG canceller noise. Under TX leakage cancellation, the CS device is protected ($\alpha_{1T} \approx 0$), and so the third-order distortion from the CS device is also minimized. From (12), we note that part of the distortion arising from the interaction between the second-order nonlinearities gets cancelled as well since $\alpha_{1T} \approx 0$ under TX leakage cancellation. Therefore, the final residual TB after TX leakage and distortion cancellation is limited by the second-order nonlinearity of the CG and the CS devices.

A complementary topology is used for the implemented LNTA (Fig. 13) for achieving high second- and third-order linearity simultaneously [36], [41]. Fig. 12 shows the simulated LNTA effective IIP_3 across TXRR. The in-band jammer and the two-tone TX leakage signal (peak power of -6 dBm) are located at 500 MHz and 600/605 MHz, respectively. The relative strength of the TX replica signal (represented by k in Fig. 11) at the gate of the CG device is swept to vary TXRR. The significance of the effective IIP_3, which is calculated from the TB, is that it represents the IIP_3 requirement that a conventional LNTA/receiver without TX leakage cancellation must achieve to have the same TB ([24])

$$\mathrm{IIP}_{3,XM} = \frac{1}{2}TB + P_{\mathrm{TX,avg}}. \tag{13}$$

In simulation, the recombination weight is chosen to satisfy the CG device and canceller noise cancellation condition [$\delta = 1$ in (12)] , so that the CG device's third-order distortion is cancelled. As shown in Fig. 12, the LNTA effective IIP_3 starts from approximately $+10$ dBm, and keeps increasing as TXRR increases until the effective IIP_3 saturates at almost $+30$ dBm, where it is limited by the finite second-order nonlinearity of the CG and CS devices. A good match between simulation and theory ((12)) is also observed. This effective IIP_3 level also agrees well with the measurements detailed later in this paper.

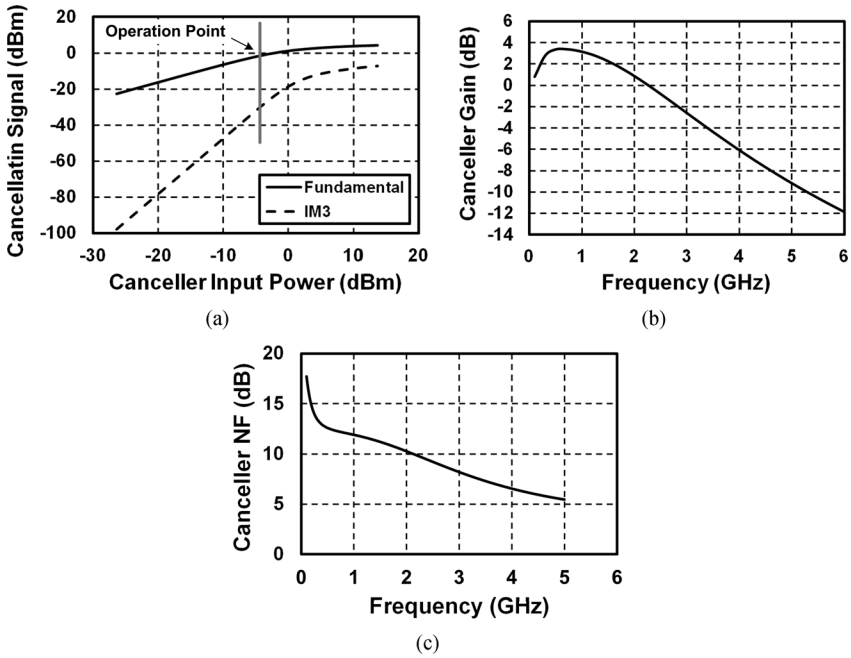

Fig. 14. Simulated CG canceller performance at the highest gain setting: (a) two-tone large signal simulation where the output cancellation signal is the current generated by the CG device, represented in terms of the incident average TX leakage power that can be cancelled, (b) ac small-signal CG canceller power gain, and (c) CG canceller NF at the RX input.

IV. Circuit Implementation

The NC-SIC receiver (Fig. 13) is implemented in 65 nm CMOS. The LNTA uses a complementary topology for high linearity as was discussed in Section III-C. The LNTA CG and CS devices are sized to have 20 mS and 80 mS transconductance, respectively. The four-phase current-driven passive mixers are driven by 25% non-overlapping LO signals and are followed by baseband Rauch TIAs [15]. eight-phase mixing [14] would lower the receiver NF further by reducing noise folding effects, and would enable harmonic rejection. The third-order Rauch TIAs offer high selectivity and low in-band impedance [15]. Large input shunt capacitors are used to help sink OOB TX leakage current in the TIAs. The Rauch TIAs in the CS path are scaled by a factor of 4 to provide the nominal CG-CS recombination weighting. In addition, programmable recombination circuits combine the receiver outputs from the CG and CS paths for noise and cross-modulation distortion cancellation. They consist of eight 5-bit binary-weighted transconductance cells for programmable complex recombination weights, as each (I/Q) receiver output is driven by 5-bit cells from the CS and CG I and Q paths. Under large TX leakage and TX noise, CG and CS cancellers are activated, respectively.

Both CG and CS cancellers adopt a Cartesian phase rotator topology which consists of two (I/Q) 6-bit variable-gain transconductance amplifiers (VGAs) as depicted in Fig. 13. For the CG canceller, an RF variable-gain TIA (VG-TIA) is inserted between the LNTA CG device and the phase rotator for gain variation and current-to-voltage conversion. Note that in the Cartesian phase rotators, the magnitude of the output current can also be modified through the VGAs at the expense of phase resolution. The phase-rotator VGAs are built using inverter-based transconductance cells for high linearity. Both

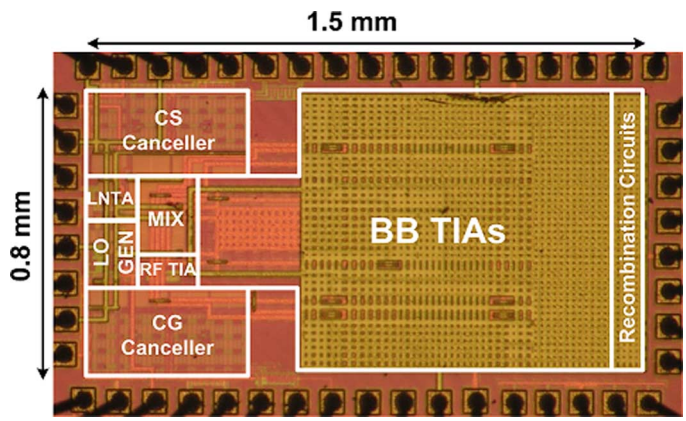

Fig. 15. Chip microphotograph of the 65 nm CMOS 0.3–1.7 GHz NC-SIC receiver.

the RF VG-TIA and the LNTA CG device use thick oxide devices to handle large TX leakage, as shown in Fig. 13. Note that the CS canceller must be designed to deliver more current than the CG canceller by a factor equal to the CS device gain (4 in our prototype). The phase rotators require broadband quadrature signal generation which has not been implemented on chip in this prototype, but the proposed low-noise active cancellation scheme eases their implementation. Passive or active polyphase filters (PPFs)[42], [43] may be employed. The loss of cascaded broadband passive PPFs can be compensated by the gain of the active canceller, while the noise of the broadband/reconfigurable active PPFs would be cancelled using the proposed scheme.

The simulated CG canceller performance is shown in Fig. 14 for peak gain setting. Fig. 14(a) depicts a two-tone simulation where the output cancellation signal is the current generated by

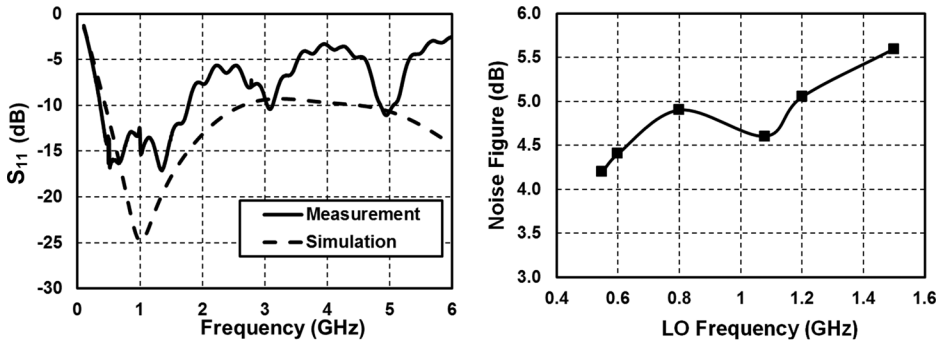

(a) (b)

Fig. 16. (a) Measured receiver S_{11} and (b) measured receiver NF across LO frequency with the cancellers inactive.

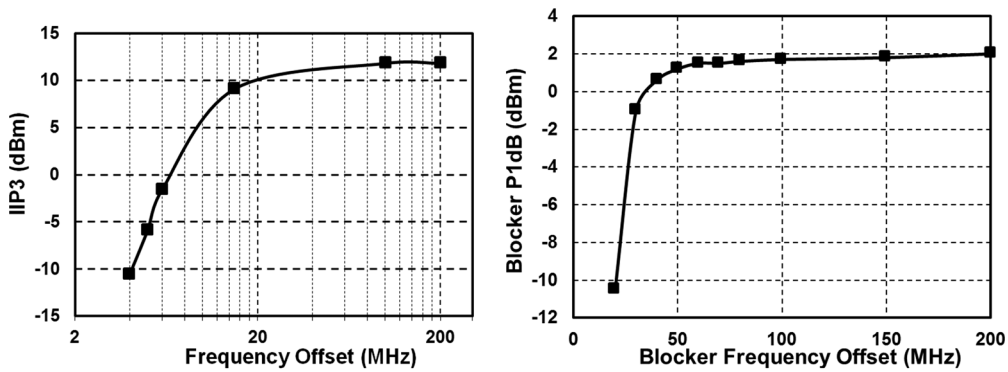

(a) (b)

Fig. 17. Measured receiver linearity with cancellers inactive. (a) Receiver IIP3 versus offset frequency of the first tone of the two-tone input and (b) receiver input-referred blocker P1 dB.

the CG device, and is represented in terms of incident average TX leakage power that can be cancelled (the peak TX leakage power is 3 dB higher). The CG canceller is able to generate a > 0 dBm cancellation signal ($+3$ dBm peak TX leakage) while generating distortion products that are less than -30 dBm. Consequently, a TXRR of more than 30 dB is achievable before the CG canceller nonlinearity starts dominating the cross-modulation performance. Fig. 14(b) shows the small-signal power gain of the CG canceller. It has a peak power gain of approximately 4 dB and a 3 dB bandwidth of approximately 2 GHz which is mainly limited by the thick oxide devices and is more than sufficient to cover the operating range. Finally, the simulated CG canceller NF is shown in Fig. 14(c).

V. Measurement Results

The chip micrograph is shown in Fig. 15. It has an active area of 1.2 mm^2. The chip is wire bonded and packaged in a 48-pin QFN package, and mounted on a 4-layer FR-4 PCB.

Generic receiver measurements are performed with both cancellers inactive, and without TX leakage. The measured and simulated receiver S_{11} is plotted in Fig. 16(a).[1] The measured receiver noise figure [Fig. 16(b)] ranges from 4.2 to 5.6 dB. The recombination weighting is optimized for NF in this measurement. Larger LNTA CS device transconductance and 8-phase mixing would further lower the receiver NF below 4.2 dB at the low end of frequency. Simulations reveal that the degradation of NF versus frequency can be mitigated by optimizing the LO path design. The receiver has a measured OOB IIP_3 of $+12$ dBm, and OOB blocker-induced P1 dB of $+2$ dBm (Fig. 17). While high OOB linearity is achieved through current-mode design, it is insufficient to tolerate > 0 dBm TX leakage (Section II-A).

Next, the receiver is measured in the presence of TX leakage and with the CG canceller active [Fig. 18(a)]. A two-tone signal with 1 MHz separation is fed into an off-the-shelf $+30$ dBm PA. Couplers are used to couple a fraction of the transmitted power to the cancellers for TX leakage and RX-band TX noise cancellation. A PCB-based planar antenna pair is used to model a coexistence environment with measured 30 dB isolation [Fig. 6(b) and (d)]. To measure cancellation at higher TX leakage levels, an attenuator-based measurement setup is also used. Approximately 30 dB suppression is measured at the receiver input across a peak leakage level ranging from -24 dBm to $+2$ dBm [Fig. 18(b)].

To demonstrate the impact of the antenna interface on the TX leakage cancellation bandwidth, the small-signal TXRR is measured across the entire TX pass-band of the Avago duplexer mentioned in Section II-C. As mentioned earlier, it should be noted that such a duplexer does not require cancellation and our work targets duplexers with reduced isolation and selectivity enabling wider cancellation BWs. Nevertheless, as shown in

[1]The difference between the measured and simulated S_{11} is due to an erroneous RF SMA connector landing pad design on the PCB.

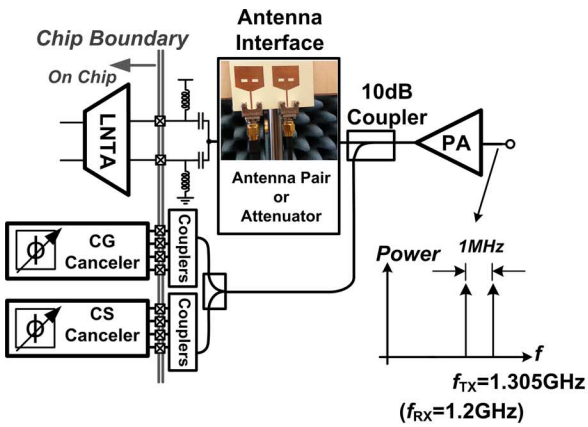

(a)

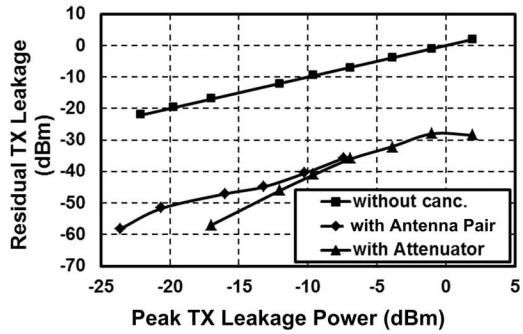

(b)

Fig. 18. (a) Setup for TX leakage cancellation measurements and (b) cancellation of TX leakage at the receiver input using the CG canceller using an antenna-pair based setup as well as an attenuator-based setup for higher leakage levels.

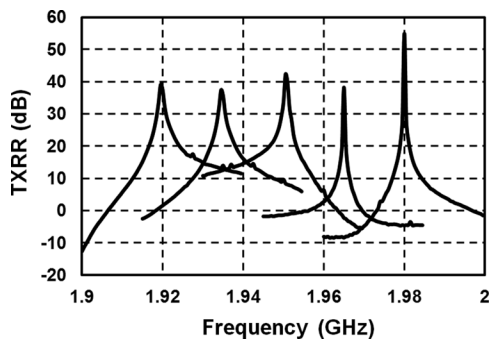

Fig. 19. Measured small-signal TXRR across the entire TX passband of the Avago ACMD-7612 miniature UMTS band-I duplexer.

in Fig. 19, the measured 20 dB TXRR cancellation bandwidth ranges from 1 to 7 MHz, with narrowest BWs observed near the band edges. This result matches reasonably well with the simulation in Section II-C.

Next, the TB is measured by introducing an in-band jammer together with the two-tone OOB TX signal. Without cancellation, reducing our receiver to a generic current-mode receiver, the TB decreases at 20 dB/decade as TX leakage power increases [Fig. 20(a)]. The effective IIP_3 (calculated from the TB using (13)) remains at +12–14 dBm, which matches the receiver OOB IIP_3 measurement shown in Fig. 17(a). Leakage cancellation is then enabled using the CG canceller. The baseband recombination circuits adjust the weights on the CG and CS paths for optimum TB performance. Currently, this adjustment is performed manually using trigonometric calculations based on the cross-modulation product levels in the individual I and Q outputs of the CG and CS paths. The TB with TX leakage cancellation remains constant at around 68 dB independent of the peak TX leakage level ranging from −22 dBm to +2 dBm [Fig. 20(b)]. The calculated receiver effective IIP_3 is as high as +33 dBm at +2 dBm peak TX leakage. These TB and effective IIP_3 levels represent enhancements of 38 dB and 19 dB, respectively, over the RX performance in the absence of cancellation.

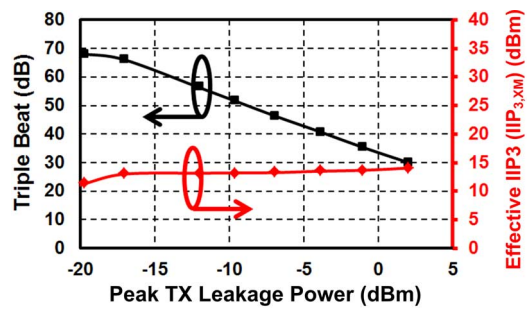

(a)

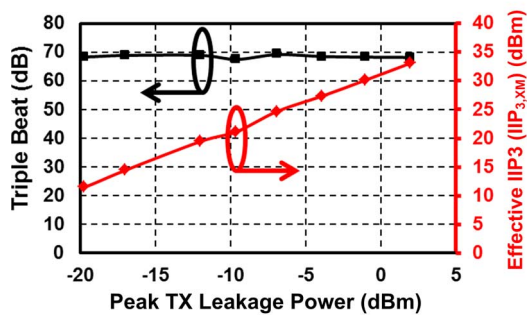

(b)

Fig. 20. Receiver triple beat and effective IIP3 measurement: (a) without cancellation and (b) with TX leakage cancellation using the CG canceller. The baseband recombination circuits adjust the weights on the CG and CS paths for optimum TB performance.

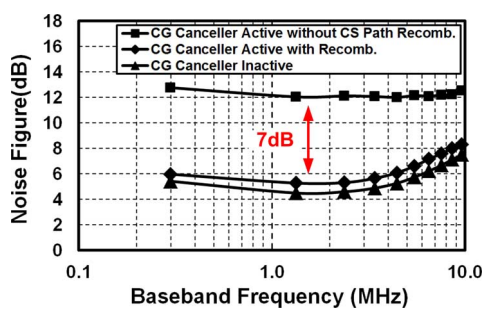

Fig. 21. Measured receiver NF without the CG canceller active, with the CG canceller active, configured for cancelling +2 dBm peak TX leakage and recombination cells configured for optimum TB performance, and with the CG canceller active but with noise cancellation disabled by turning off the recombination circuits in the CS path.

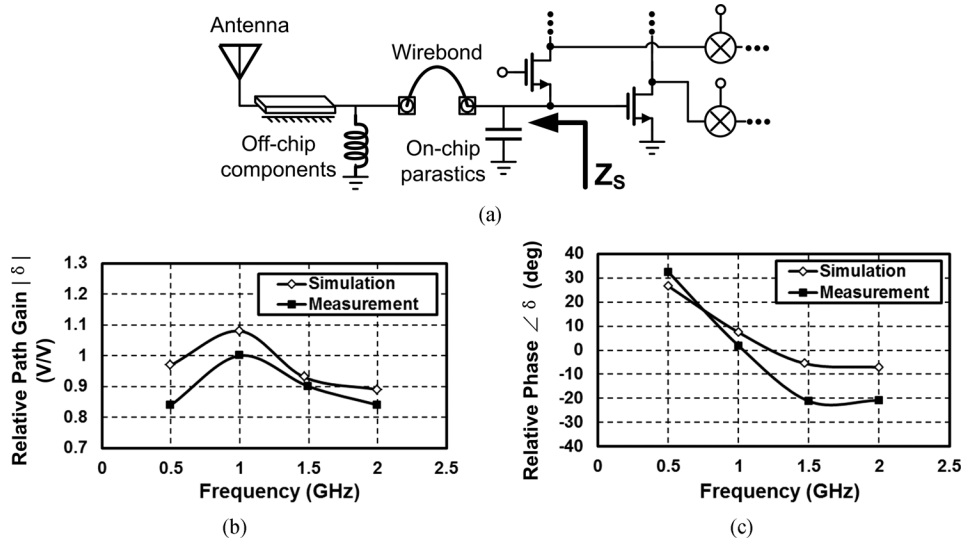

Fig. 22. (a) Mechanisms of variation in source impedance. (b) Measured and simulated relative path gain in the baseband recombination cells for optimum noise performance of the receiver with CG canceller active and configured for maximum gain across frequency. (c) Measured and simulated relative phase adjustment in the baseband recombination cells for optimum noise performance.

Fig. 21 shows the receiver NF when the CG-canceller is active and configured for cancelling +2 dBm peak TX leakage. The recombination cells are also configured for optimum TB performance as was the case for Fig. 20(b). The noise figure degradation is less than 0.8 dB when compared to the receiver with the canceller disabled and with recombination cells configured for optimum NF. The analyses in Sections III-B and III-C quantify the achievable TB when the recombination is configured for optimum NF, but here we have measured the NF when the recombination is configured for optimum TB since TB typically limits the sensitivity in the presence of strong modulated TX leakage. Hence, the NF increase is slightly higher than the theoretical result in Section III-B. In addition, the receiver noise figure with the CG canceller active but with noise cancellation disabled by turning off the recombination circuits in the CS path is measured. The noise figure is degraded by almost 7 dB, representing the penalty of performing active cancellation at the receiver input without our approach.

The leakage, noise and cross-modulation cancellation have a dependence on the source impedance, which can deviate from 50 Ω due to on-chip and package parasitics, off-chip biasing components, as well as variations in the antenna impedance [Fig. 22(a)]. The recombination condition for optimum receiver NF across frequency with CG canceller active and configured for maximum gain is measured to quantify the impact of the varying source impedance caused by package parasitics and off-chip biasing components [Fig. 22(b) and (c)]. The optimum relative path gain for overall receiver NF is close to the nominal condition with less than 20% variation, while the optimal relative path phase varies from 32 to −22 degrees. They are relatively robust with respect to varying source impedance, and closely match simulations. While antenna tuner modules (ATMs) [44] somewhat limit antenna impedance variation, it is expected that adaptive digital calibration techniques will be required in practical scenarios.

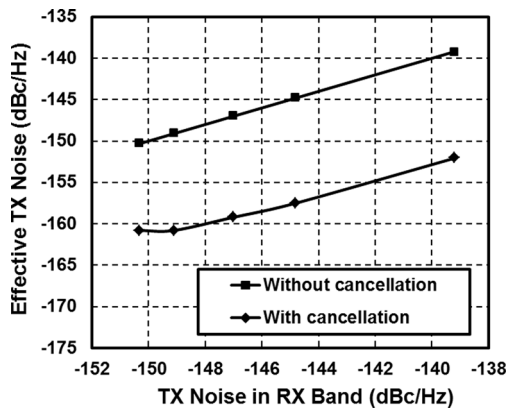

Fig. 23. Measured TX noise cancellation results when both CG and CS cancellers are activated. The TX leakage is fixed at −6 dBm peak power with varying RX-band noise level.

Finally, both CG and CS cancellers are activated for simultaneous TX leakage and TX noise cancellation. The TX leakage is fixed at −6 dBm peak power[2] with varying RX-band noise level. The effective TX noise in the RX band after cancellation is computed from the measured total receiver noise after subtracting the contribution of the receiver itself. The CS-canceller's noise is not subtracted for a fair calculation. From Fig. 23, despite the CS canceller adding noise, up to 13 dB reduction of effective TX noise in the RX band is observed.

Table I summarizes the performance of the proposed receiver. When compared with the receivers with TX leakage cancellation or suppression, our work exhibits wider operation bandwidth, higher OOB linearity and 30 dB improvement in maximum handled TX leakage with less than 0.8 dB noise

[2]The reduced TX leakage power level in this measurement is partly due to the measurement setup and partly due to the current delivery capability of the CS canceller. An auxiliary current-mode downconversion path for the cancellation of PA noise (similar to [38]) with independent baseband gain control would enable power-efficient cancellation at higher power levels.

TABLE I
PERFORMANCE SUMMARY AND COMPARISON WITH THE STATE OF THE ART

	[24]	[25]	[9]	[10]	[15]	This work
Architecture	TX Leakage Cancellation/Suppression		Highly-Linear Software-Defined Radio			Current-Mode Receiver with active two-point low-noise TX-leakage cancellation.
	Active TX Leakage Suppression After LNA	Active TX Leakage Cancellation After LNA	High Linearity Passive Mixer-First	Mixer First with Distortion Cancellation	Current-Mode RX with Highly-Linear LNTA	
CMOS Technology	180nm	250nm	65nm	65nm	40nm	65nm
RF Frequency	1.96GHz	800MHz	0.1-2.4GHz	0.2-2.6GHz	1.8-2.4(TDD)/ 1.8-2.1(FDD) GHz	0.3-1.7GHz
Gain	45dB	14.8dB (LNA)	40-70dB	26.5dB	45.5dB	19-34dB
Baseband BW	N/A	N/A	20MHz[1]	12MHz	1.4(TDD)/ 3.4(FDD) MHz	2-76MHz
DSB NF	3.1dB	1.4dB (LNA)	4dB	7.5dB	3.8(TDD)/ 3.1(FDD) dB	4.2dB
Blocker P1dB	N/A	N/A	+4dBm[2]	N/A	N/A	>+2dBm[3]
Out-of-band IIP3	N/A	N/A	+25dBm	+10/+18dBm[4]	+18(TDD)/ +16(FDD) dBm	+12dBm/+33dBm[5]
Maximum Handled Peak TX Leakage	-28dBm[6]	-28dBm[7]	N/A	N/A	N/A	+2dBm[6]
NF Degradation due to Leakage Cancellation	1.8dB	1.3dB (LNA)	N/A	N/A	N/A	<0.8dB
TB_{2dBm}[8]	9dB[9]	N/A	52dB[10]	22/38dB[10]	38(TDD)/ 34(FDD) dB[10]	30dB (without cancellation) 68dB (with cancellation)
TX Noise Cancellation	N/A	N/A	N/A	N/A	N/A	13dB
RX Power Consumption	114mW	N/A	37-70mW	17.3-36.7mW	30.7mW	74.6-83.0mW
Canceller Power Consumption	48mW	43mW	N/A	N/A	N/A	13-72mW
Active Area	N/A	N/A	2mm²	0.2 mm²	0.74 mm²	1.2 mm²

[1] Maximum BW [2] Blocker at 40MHz offset [3] Blocker at >60MHz offset [4] First tone at 135MHz/>450MHz offset
[5] Effective IIP3 for TX leakage under cancellation of +2dBm peak TX leakage [6] 3dB Peak-to-average ratio
[7] 6dB Peak-to-average ratio [8] Triple beat at +2dBm peak TX leakage power [9] Calculated from reported TB at -28dBm TX leakage level
[10] Calculated from reported IIP3 (IIP3=0.5×TB+$P_{TX,avg}$ [6]) *Metrics related to the TX leakage cancellation are highlighted with*

figure degradation. The NF degradation is even smaller than prior works where the TX leakage is 30 dB weaker. When compared with highly linear software-defined receivers, our work has higher OOB linearity in the face of powerful modulated TX leakage. Finally, our work also alleviates the TX's RX-band noise requirement.

VI. CONCLUSION

A low-noise active TX leakage cancellation technique is proposed that embeds the cancellation circuitry in a noise-cancelling LNTA so that the noise and the distortion of the cancellation circuitry are cancelled. The technique can be more generally viewed as an active combining structure that has ideally no noise penalty, and is able to handle large signals without generating distortion. While applied here for TX leakage cancellation, it can be applied to any scenario where a replica of an interference signal can be generated. A second injection point is used for TX noise cancellation, and its noise impact is reduced by the RF gain. Cancellation bandwidth in self-interference cancellation is typically limited by the antenna interface selectivity. Replicating the antenna interface transfer function on chip (in other words, creating a faithful TX leakage replica) for wideband cancellation is a topic for future research. Adaptive digital calibration techniques that ensure cancellation across factors such as time-varying source impedance are also of interest.

ACKNOWLEDGMENT

The authors would like to thank Dr. B. Chappell of DARPA and Dr. P. Watson of AFRL for discussions and feedback. The authors would like to thank J. Zhu from CISL and other group members from CoSMIC lab for discussions, support and assistance. The authors would also like to acknowledge the anonymous reviewers for valuable comments that have improved the quality of the manuscript.

REFERENCES

[1] A. El Oualkadi, M. El Kaamouchi, J.-M. Paillot, D. Vanhoenacker-Janvier, and D. Flandre, "Fully integrated high-Q switched capacitor bandpass filter with center frequency and bandwidth tuning," in *Proc. IEEE RFIC Symp.*, Jun. 2007, pp. 681–684.

[2] A. Mirzaei, H. Darabi, A. Yazdi, Z. Zhou, E. Chang, and P. Suri, "A 65 nm CMOS quad-band SAW-less receiver SoC for GSM/GPRS/EDGE," *IEEE J. Solid-State Circuits*, vol. 46, no. 4, pp. 950–964, Apr. 2011.

[3] A. Ghaffari, E. Klumperink, M. C. M. Soer, and B. Nauta, "Tunable high-q N-path band-pass filters: Modeling and verification," *IEEE J. Solid-State Circuits*, vol. 46, no. 5, pp. 998–1010, May 2011.

[4] A. Mirzaei, H. Darabi, and D. Murphy, "A low-power process-scalable super-heterodyne receiver with integrated high-Q filters," *IEEE J. Solid-State Circuits*, vol. 46, no. 12, pp. 2920–2932, Dec. 2011.

[5] A. Mirzaei, H. Darabi, and D. Murphy, "Architectural evolution of integrated m-phase high-Q bandpass filters," *IEEE Trans. Circuits Syst. I, Reg. Papers*, vol. 59, no. 1, pp. 52–65, Jan. 2012.

[6] M. Darvishi, R. van der Zee, E. Klumperink, and B. Nauta, "Widely tunable 4th order switched g_m-c band-pass filter based on N-path filters," *IEEE J. Solid-State Circuits*, vol. 47, no. 12, pp. 3105–3119, Dec. 2012.

[7] M. Darvishi, R. van der Zee, and B. Nauta, "Design of active N-path filters," *IEEE J. Solid-State Circuits*, vol. 48, no. 12, pp. 2962–2976, Dec. 2013.

[8] M. Soer, E. Klumperink, Z. Ru, F. van Vliet, and B. Nauta, "A 0.2-to-2.0 GHz 65 nm CMOS receiver without LNA achieving $>$ 11 dBm IIP3 and $<$ 6.5 dB nF," in *IEEE Int. Solid-State Circuits Conf. Dig. Techn. Papers*, Feb. 2009, pp. 222–223.

[9] C. Andrews and A. Molnar, "A passive mixer-first receiver with digitally controlled and widely tunable RF interface," *IEEE J. Solid-State Circuits*, vol. 45, no. 12, pp. 2696–2708, Dec. 2010.

[10] D. Mahrof, E. Klumperink, M. Oude Alink, and B. Nauta, "A receiver with in-band IIP3 $>$ 20 dBm, exploiting cancelling of opamp finite-gain-induced distortion via negative conductance," in *Proc. IEEE RFIC Symp.*, Jun. 2013, pp. 85–88.

[11] J. Borremans, G. Mandal, V. Giannini, B. Debaillie, M. Ingels, T. Sano, B. Verbruggen, and J. Craninckx, "A 40 nm CMOS 0.4–6 GHz receiver resilient to out-of-band blockers," *IEEE J. Solid-State Circuits*, vol. 46, no. 7, pp. 1659–1671, Jul. 2011.

[12] Z. Ru, N. Moseley, E. A. M. Klumperink, and B. Nauta, "Digitally enhanced software-defined radio receiver robust to out-of-band interference," *IEEE J. Solid-State Circuits*, vol. 44, no. 12, pp. 3359–3375, Dec. 2009.

[13] C.-Y. Yu, I. Lu, Y.-H. Chen, L.-C. Cho, C. Sun, C.-C. Tang, H.-H. Chang, W.-C. Lee, S.-J. Huang, T.-H. Wu, C.-S. Chiu, and G. Chien, "A SAW-less GSM/GPRS/EDGE receiver embedded in 65-nm SoC," *IEEE J. Solid-State Circuits*, vol. 46, no. 12, pp. 3047–3060, Dec. 2011.

[14] D. Murphy, H. Darabi, A. Abidi, A. Hafez, A. Mirzaei, M. Mikhemar, and M.-C. Chang, "A blocker-tolerant, noise-cancelling receiver suitable for wideband wireless applications," *IEEE J. Solid-State Circuits*, vol. 47, no. 12, pp. 2943–2963, Dec. 2012.

[15] I. Fabiano, M. Sosio, A. Liscidini, and R. Castello, "SAW-less analog front-end receivers for TDD and FDD," *IEEE J. Solid-State Circuits*, vol. 48, no. 12, pp. 3067–3079, Dec. 2013.

[16] H. Darabi, "A blocker filtering technique for SAW-less wireless receivers," *IEEE J. Solid-State Circuits*, vol. 42, no. 12, pp. 2766–2773, Dec. 2007.

[17] S. Ayazian and R. Gharpurey, "Feedforward interference cancellation in radio receiver front-ends," *IEEE Trans. Circuits Syst. II, Exp. Briefs*, vol. 54, no. 10, pp. 902–906, Oct. 2007.

[18] A. Balankutty and P. Kinget, "An ultra-low voltage, low-noise, high linearity 900-MHz receiver with digitally calibrated in-band feed-forward interferer cancellation in 65-nm CMOS," *IEEE J. Solid-State Circuits*, vol. 46, no. 10, pp. 2268–2283, Oct. 2011.

[19] A. Safarian, A. Shameli, A. Rofougaran, M. Rofougaran, and F. De Flaviis, "Integrated blocker filtering RF front ends," in *Proc. IEEE RFIC) Symp.*, Jun. 2007, pp. 13–16.

[20] J. Park and B. Razavi, "A 20 mW GSM/WCDMA receiver with RF channel selection," in *IEEE Int. Solid-State Circuits Conf. Dig. Techn. Papers*, Feb. 2014, pp. 356–357,357a.

[21] H. Joshi, H. H. Sigmarsson, S. Moon, D. Peroulis, and W. Chappell, "Tunable high Q narrow-band triplexer," in *IEEE MTT-S Int. Microw. Symp. Dig.*, Jun. 2009, pp. 1477–1480.

[22] Y.-H. Kuo, J.-H. Tsai, and T.-W. Huang, "A digital-calibrated transmitter-to-receiver isolator in radar applications," *IEEE Microw. Wireless Compon. Lett.*, vol. 22, no. 12, pp. 651–653, Dec. 2012.

[23] N. Kim, L. Larson, and V. Aparin, "A highly linear SAW-less CMOS receiver using a mixer with embedded TX filtering for CDMA," *IEEE J. Solid-State Circuits*, vol. 44, no. 8, pp. 2126–2137, Aug. 2009.

[24] H. Khatri, P. Gudem, and L. Larson, "An active transmitter leakage suppression technique for CMOS SAW-less CDMA receivers," *Solid-State Circuits, IEEE J. of*, vol. 45, no. 8, pp. 1590–1601, 2010.

[25] V. Aparin, G. Ballantyne, C. Persico, and A. Cicalini, "An integrated LMS adaptive filter of TX leakage for CDMA receiver front ends," *IEEE J. Solid-State Circuits*, vol. 41, no. 5, pp. 1171–1182, May 2006.

[26] V. Aparin, "A new method of TX leakage cancelation in W/CDMA and GPS receivers," in *Prof. IEEE RFIC Symp.*, Jun. 2008, pp. 87–90.

[27] J. Zhou, P. Kinget, and H. Krishnaswamy, "A blocker-resilient wideband receiver with low-noise active two-point cancellation of $>$ 0 dBm TX leakage and TX noise in RX band for FDD/co-existence," in *IEEE Int. Solid-State Circuits Conf. Dig. Techn. Papers*, Feb. 2014, pp. 352–353.

[28] V. Aparin and L. Larson, "Analysis and reduction of cross-modulation distortion in CDMA receivers," *IEEE Trans. Microw. Theory Techn.*, vol. 51, no. 5, pp. 1591–1602, May 2003.

[29] N. Swanberg, J. Phelps, and M. Recouly, "WCDMA cross modulation effects and implications for receiver linearity requirements," in *Prof. IEEE Radio Wireless Conf.*, 2002, pp. 13–18.

[30] B. Razavi, *RF Microelectronics*, 2nd ed. London, U.K.: Pearson, 2011.

[31] *"Skyfr-000709 Miniature 2110–2170 MHz Single Junction Robust Lead Circulator Data Sheet,"* Skyworks Solutions, Woburn, MA, USA.

[32] Z. N. Low, J. H. Cheong, and C. L. Law, "Low-cost PCB antenna for low-cost PCB antenna for UWB applications," *Antennas Wireless Propagat. Lett.*, vol. 4, no. 1, pp. 237–239, Dec. 2005.

[33] *"ACMD-7612 Miniature UMTS Band i Duplexer Data Sheet,"* Avago Technol., San Jose, CA, USA.

[34] F. Bruccoleri, E. Klumperink, and B. Nauta, "Wide-band CMOS low-noise amplifier exploiting thermal noise canceling," *IEEE J. Solid-State Circuits*, vol. 39, no. 2, pp. 275–282, Feb. 2004.

[35] S. Blaakmeer, E. Klumperink, D. Leenaerts, and B. Nauta, "Wideband balun-LNA with simultaneous output balancing, noise-canceling and distortion-canceling," *IEEE J. Solid-State Circuits*, vol. 43, no. 6, pp. 1341–1350, Jun. 2008.

[36] J. Zhu, H. Krishnaswamy, and P. R. Kinget, "Field-programmable LNAs with interferer-reflecting loop for input linearity enhancement," *IEEE J. Solid-State Circuits*, submitted for publication.

[37] W.-H. Chen, G. Liu, B. Zdravko, and A. Niknejad, "A highly linear broadband CMOS LNA employing noise and distortion cancellation," *IEEE J. Solid-State Circuits*, vol. 43, no. 5, pp. 1164–1176, May 2008.

[38] M. Omer, R. Rimini, P. Heidmann, and J. S. Kenney, "A PA-noise cancellation technique for next generation highly integrated RF front-ends," in *Proc. IEEE RFIC Symp.*, Jun. 2012, pp. 471–474.

[39] D. Kaczman, M. Shah, M. Alam, M. Rachedine, D. Cashen, L. Han, and A. Raghavan, "A single chip 10-band WCDMA/HSDPA 4-band GSM/EDGE SAW-less CMOS receiver with DIGRF 3G interface and $+90$ dBm IIP2," *IEEE J. Solid-State Circuits*, vol. 44, no. 3, pp. 718–739, Mar. 2009.

[40] Y. Feng, G. Takemura, S. Kawaguchi, N. Itoh, and P. Kinget, "Digitally assisted IIP2 calibration for CMOS direct-conversion receivers," *IEEE J. Solid-State Circuits*, vol. 46, no. 10, pp. 2253–2267, Oct. 2011.

[41] H. Zhang and E. Sanchez-Sinencio, "Linearization techniques for CMOS low noise amplifiers: A tutorial," *IEEE Trans. Circuits Syst. I, Reg. Papers*, vol. 58, no. 1, pp. 22–36, Jan. 2011.

[42] M. Kaltiokallio and J. Ryynnen, "A 1 to 5 GHz adjustable active polyphase filter for LO quadrature generation," in *Proc. IEEE RFIC Symp.*, Jun. 2011, pp. 1–4.

[43] J. Kaukovuori, K. Stadius, J. Ryynanen, and K. A. I. Halonen, "Analysis and design of passive polyphase filters," *IEEE Trans. Circuits Syst. I, Reg. Papers*, vol. 55, no. 10, pp. 3023–3037, Nov. 2008.

[44] M. de Jongh, A. van Bezooijen, T. Bakker, K. Boyle, and J. Stulemeijer, "A low-cost closed-loop antenna tuner module for mobile phone single-feed multi-band antennas," in *Proc. Eur. Microw. Conf.*, Oct. 2013, pp. 1171–1174.

Jin Zhou (S'11) received the B.S. degree in electronics science and technology from Wuhan University, Wuhan, China, in 2008, and the M.S. degree in microelectronics from Fudan University, Shanghai, China, in 2011. He is currently working toward the Ph.D. degree at Columbia University, New York, NY, USA.

From 2008 to 2011, he was a research assistant at Fudan University, designing frequency synthesizer for multi-standard wireless communication system. From 2011 to 2012, he was with MediaTek Singapore as a RFIC design engineer working on PLL, DLL for cellular and wireless products.

Anandaroop Chakrabarti (S'12) received the B.Tech. degree in electronics and electrical communication engineering from the Indian Institute of Technology, Kharagpur, India, in 2010, and the M.S. degree in electrical engineering from Columbia University, New York, NY, USA, in 2011, where he is currently working toward the Ph.D. degree.

He spent the summers of 2013 and 2014 as an Intern with IBM T. J. Watson Research Center working on W-band PAs and low phase-noise millimeter-wave (mm-wave) VCOs. His research interests include mm-wave and RF circuits and systems in silicon, massive mm-wave multi-input-multi-output systems, and related applications.

Peter R. Kinget (M'90–SM'02–F'11) received the engineering degree (*summa cum laude*) in electrical and mechanical engineering and Ph.D. degree (*summa cum laude* with Congratulations of the Jury) in electrical engineering from the Katholieke Universiteit Leuven, Leuven, Belgium, in 1990 and 1996, respectively.

From 1991 to 1995, he received a graduate fellowship from the Belgian National Fund for Scientific Research (NFWO) and was a Research Assistant with the ESAT-MICAS Laboratory of the Katholieke Universiteit Leuven. From 1996 to 1999, he was with Bell Laboratories, Lucent Technologies, Murray Hill, NJ, USA, as a Member of Technical Staff in the Design Principles Department. From 1999 to 2002, he held various technical and management positions in IC design and development at Broadcom, CeLight, and MultiLink. In 2002, he joined the faculty of the Department of Electrical Engineering, Columbia University, New York, NY, USA. During 2010–2011, he was with the Université catholique de Louvain, Belgium, on sabbatical leave. He also serves as an expert on patent litigation and a technical consultant to industry. His research interests are in analog, RF, and power integrated circuits and the applications they enable in communications, sensing, and power management. He is widely published in circuits and systems journals and conferences, has coauthored three books, and holds 16 U.S. patents with several applications under review. His research group has received funding from the National Science Foundation, the Semiconductor Research Corporation, the Department of Energy (ARPA-E), the Department of Defense (DARPA), and an IBM Faculty Award. It has further received in-kind and grant support from several of the major semiconductor companies.

Dr. Kinget is an elected member of the IEEE Solid-State Circuits Adcom (2011–2013 and 2014–2017). He has been an IEEE Distinguished Lecturer of the IEEE Solid-State Circuits Society (2009–2010) and an associate editor of the IEEE JOURNAL OF SOLID STATE CIRCUITS (2003–2007) and the IEEE TRANSACTIONS ON CIRCUITS AND SYSTEMS II (2008–2009). He has served as a member of the Technical Program Committee of the IEEE Custom Integrated Circuits Conference (2000–2005), the Symposium on VLSI Circuits (2003–2006), the European Solid-State Circuits Conference (2005–2010) and the International Solid-State Circuits Conference (2005–2012). He was a corecipient of several awards, including the Best Student Paper Award—1st Place at the 2008 IEEE Radio Frequency Integrated Circuits (RFIC) Symposium, the First Prize in the 2009 Vodafone Americas Foundation Wireless Innovation Challenge, the Best Student Demo Award at the 2011 ACM Conference on Embedded Networked Sensor Systems (ACM SenSys), the 2011 IEEE Communications Society Award for Advances in Communications, and the "First Prize ($100 K)" in the 2012 Interdigital Wireless Innovation Challenge (I2C).

Harish Krishnaswamy (S'03–M'09) received the B.Tech. degree from the Indian Institute of Technology, Madras, India, in 2001, and the M.S. and Ph.D. degrees from the University of Southern California, Los Angeles, CA, USA, in 2003 and 2009, respectively, all in electrical engineering.

In 2009, he joined the Electrical Engineering Department, Columbia University, New York, NY, USA, as an Assistant Professor. His research interests broadly span integrated devices, circuits, and systems for a variety of RF, mm-wave, and sub-mm-wave applications. His current research efforts are focused on silicon-based mm-wave PAs, sub-mm-wave circuits and systems, reconfigurable/broadband RF transceivers for cognitive and software-defined radio, full-duplex radios, and circuits and systems for massive mm-wave MIMO communication. His research group has received funding from various federal agencies, including NSF and DARPA, as well as industry. He also serves as a technical consultant to industry.

Prof. Krishnaswamy serves as a member of the Technical Program Committee (TPC) of several conferences, including the IEEE RFIC Symposium. He was the recipient of the IEEE International Solid-State Circuits Conference (ISSCC) Lewis Winner Award for Outstanding Paper in 2007, the Best Thesis in Experimental Research Award from the USC Viterbi School of Engineering in 2009, the Defense Advanced Research Projects Agency (DARPA) Young Faculty Award in 2011, and a 2014 IBM Faculty Award.